ACS OMEGA

http://pubs.acs.org/journal/acsodf

Article

Novel Gastroprotective and Thermostable Cocrystal of Dimethyl Fumarate: Its Preparation, Characterization, and *In Vitro* and *In Vivo* Evaluation

Qadir Alam, Ankit Ganeshpurkar, Sushil Kumar Singh, and Sairam Krishnamurthy*

Cite This: *ACS Omega* 2023, 8, 26218−26230

Read Online

ACCESS | Metrics & More | Article Recommendations | Supporting Information

ABSTRACT: Crystallization has revolutionized the field of solid-state formulations by modulating the physiochemical and release profile of active pharmaceutical ingredients (APIs). Dimethyl fumarate (DF), an FDA-approved first-line drug for relapsing−remitting multiple sclerosis, has a sublimation problem, leading to loss of the drug during its processing. To tackle this problem, DF cocrystal has been prepared by using solvent evaporation technique using nicotinamide as a coformer, which has been chosen based on *in silico* predictions and their ability to participate in hydrogen bonding. Fourier transform infrared (FT-IR), powder X-ray diffraction (PXRD), thermogravimetric analysis (TGA), differential scanning calorimetry (DSC), and sublimation analysis have characterized the cocrystal and its thermostability. Comparative analysis of the release profile has been done by the dissolution and pharmacokinetic study of DF and its cocrystal. Formulated cocrystal is noncytotoxic, antioxidant and inhibits interleukin-6 and tissue necrosis factor-α in peripheral blood mononuclear cells induced by lipopolysaccharide. We have obtained a thermostable cocrystal of DF with a similar physicochemical and release profile to that of DF. The formulated cocrystal also provides a gastroprotective effect which helps counterbalance the adverse effects of DF by reducing lipid peroxidation and total nitrite levels.

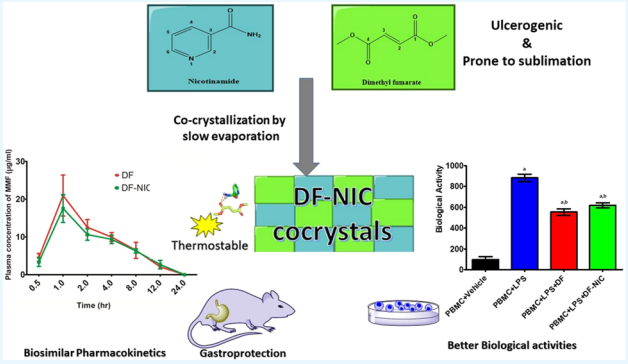

INTRODUCTION

Dimethyl fumarate (DF) is an FDA-approved drug for treating relapsing−remitting multiple sclerosis and psoriasis. It has antioxidant, anti-inflammatory, and immunomodulatory properties, which contribute to its efficacy in various diseases.[1] It is available as an oral drug in tablet and capsule formulation, and after ingestion, it is hydrolyzed into an active metabolite-monomethylfumarate (MMF). DF has a physiochemical disadvantage as it sublimates at a relatively low temperature, when processed conventionally; about 15−20% of DF is lost from the final formulation.[2] This is most likely because of sublimation of DF during production. Sublimation also leads to the loss of DF during long-term storage from bulk and its formulations as well, and the capsule formulation containing DF needs to be discarded within 90 days after the bottle of the capsule is opened.[3] Moreover, DF owes some serious gastrointestinal (GI) adverse effects like anal incontinence, diarrhea, dyspepsia, irritable bowel syndrome, gastritis, erosive gastritis, gastric ulcer, and gastroduodenitis.[4,5]

Cocrystals have been used to improve thermodynamic stability[6] and physicochemical properties like the solubility and dissolution profile of the drugs.[7] A cocrystal denotes two or more molecules that have been combined into the same crystal lattice through intermolecular interactions like hydrogen bonding, p−p stacking, and van der Waals forces with a fixed stoichiometric ratio, creating a special multicomponent supramolecular crystal structure. Cocrystals comprise active pharmaceutical ingredients (APIs) and benign molecules or other APIs as coformers[8] via hydrogen bond interactions.[9] As hydrogen bonds rely on hydrogen bond donor and acceptor characteristics of functional groups, coformers are selected cautiously based on the nature of the API. It is also essential to establish whether a reaction between an API and a coformer will result in a cocrystal or salt formation.[10] Salt or cocrystal formation can be predicted from the pK_a values of the coformer and API being chosen.[11] The supramolecular synthon approach, which utilizes the Cambridge structural database (CSD) to effectively prioritize coformers for crystal form screening, is another useful tool for making cocrystals.[12] DF has four hydrogen bond acceptors measured using Cactvs 3.4.6.11 (PubChem release 2019.06.18), which makes it a

Received: April 11, 2023
Accepted: June 22, 2023
Published: July 11, 2023

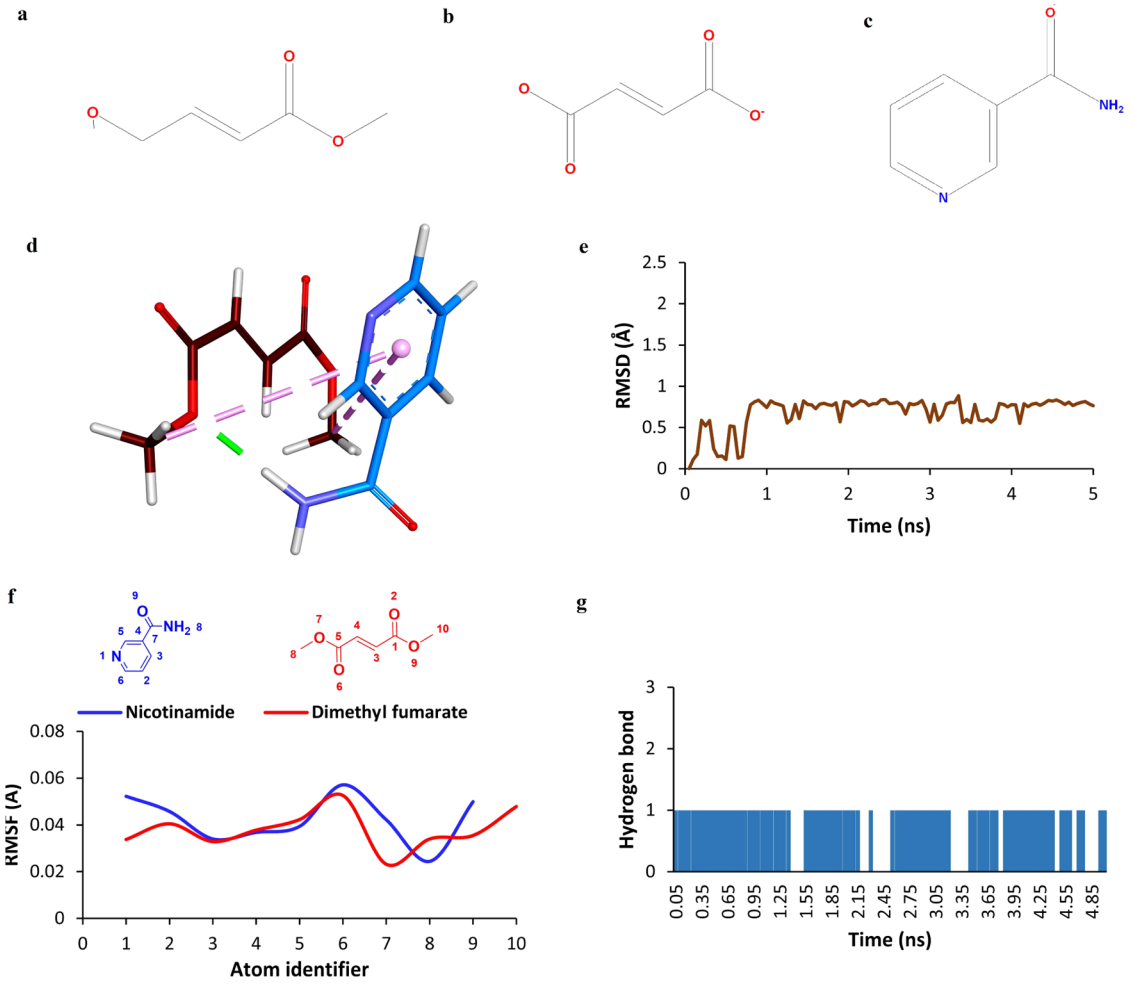

Figure 1. (a) Molecular structure of DF, (b) molecular structure of MMF, (c) molecular structure of NIC, (d) the 3D interaction between DF and NIC, (e) RMSD of the system, (f) RMSF of the atoms of DF and NIC, and (g) the number of hydrogen bonds between DF and NIC w.r.t. time.

potential molecule to undergo cocrystallization. Cocrystals of DF with gentisic acid and camphoric acid have been reported to show enhanced absorption and bioavailability.[13] Nicotinamide (NIC) has been used extensively as a coformer to make cocrystals for altering the physicochemical properties of many drugs.[14] NIC, a coformer, possesses a single hydrogen bond donor with two acceptor counts, as computed by Cactvs 3.4.6.11 (PubChem release 2019.06.18). Nicotinamide possesses a cytoprotective effect against indomethacin-induced gastric lesions due to its antioxidant property and its ability to restore gastric mucus and nitric oxide contents and attenuate the enhanced gastric microvascular permeability.[15] Cocrystals can be made from a plethora of methods, including liquid-assisted grinding, slurry conversion, supercritical fluid method, and solution method. We have utilized the solvent evaporation method due to its high efficacy and reproducibility of cocrystallization.[16] This technique involves the nucleation and growth of cocrystals from a solution containing coformers and APIs with loss of the solvent via evaporation of the solvent. In the solvent evaporation method, the size of the crystals can be controlled by modulating the rate of evaporation of the solvent, providing it an edge over other methods of cocrystallization.[17]

DF is a prodrug with monomethylfumarate (MMF) as its primary metabolite,[18] but many studies have shown DF to exert a more cytoprotective effect than MMF.[19] Once absorbed, DF/MMF rapidly penetrates blood cells, mainly peripheral blood mononuclear cells (PBMC), and covalently binds to glutathione (GSH) and other molecules.[20] PBMC analysis is one of the important parameters to evaluate the pharmacological actions of DF, and lipopolysaccharide (LPS)-induced inflammation in PBMC has been utilized in this work to evaluate the anti-inflammatory activity of DF and formulated cocrystal.[21] Moreover, DF is well known to decrease the synthesis of proinflammatory mediators like tumor necrosis factor-α (TNF-α), interleukin-1β (IL-1β), reactive oxygen species (ROS), and interleukin-6 (IL-6) in activated microglia and astrocytes and LPS-activated PBMCs,[22] so we have evaluated the effect of DF and cocrystal on the change in intracellular ROS and TNF-α and IL-6 activity in LPS-induced PBMC.

Sublimation-mediated loss of DF and its gastric-related adverse effects have motivated us to formulate its cocrystal using NIC as a coformer. We have characterized the cocrystal using thermal stability indicators such as differential scanning calorimetry (DSC), thermogravimetric analysis (TGA), and thermal assault. Spectral tools like Fourier transform infrared (FTIR) and powder X-ray diffraction (PXRD) are important tools to characterize cocrystallization. To evaluate the thermostability of the cocrystals, we have exposed DF and the formulated cocrystal to an extreme condition of 60 °C and 75% relative humidity (RH) for 20 days. We have compared

https://doi.org/10.1021/acsomega.3c02463
ACS Omega 2023, 8, 26218−26230

DF and its formulated cocrystal for *in vitro* cytotoxicity LPS-induced alterations in ROS, IL-6, and TNF-α in PBMC. We have also performed *in vitro* dissolution and *in vivo* pharmacokinetic profiling of DF and the cocrystal. The gastroprotective effect of the cocrystal has been evaluated against the acute ulcer model and acetic acid-induced ulcer healing model.

RESULTS AND DISCUSSION

Molecular Docking. The docking was employed for the identification of the preferable poses of the interacting coformers, *i.e.*, DF and NIC, in the obtained cocrystal. A Lamarckian genetic algorithm was employed for the generation of the various poses, which were further evaluated through the semiempirical free-energy force field-based scoring function of AutoDock-4.2.6. It was observed that the docking pose displayed a hydrogen bond between the hydrogen of the amino group of NIC and one of the oxygens, which contributed to the ester bond of DF. Further, the length of the hydrogen bond was found to be 1.89 Å, with a bond energy of −7.523 Kcal/mol, indicating the strength of the bond. It was also observed that both terminal methyl groups of DF displayed π-alkyl interactions with the phenyl ring of NIC (Figure 1).

Molecular Dynamics. The molecular dynamics (MD) study was carried out to access the stability of the interactions between the coformer units with the help of AMBER 20. A positional restrain force of 10,000 Kcal/mol was applied to mimic the interstitial force experienced by the unit cell of a crystal.[23] A 5 ns isobaric isothermal ensemble (NPT) MD simulation confirmed the stable interaction of DF and NIC moieties. Root-mean-square deviation (RMSD) is the indicator of the mean positional deviation of a group of atoms compared to a given frame. The RMSD value of the cocrystal unit was found to be stable, except for the initial 1 ns of the run. The mean RMSD was found to be 0.682 ± 0.196 Å. Further, the mean RMSD for 1−5 ns was found to be 0.748 ± 0.087 Å. The lower value of the standard deviation across this period indicated stable interactions. The fluctuation about a single atom for the complete simulation time could be measured through root-mean-square fluctuation (RMSF). The RMSF of all of the atoms of both molecules was below 1 Å, which is quite low. Further, the nitrogen atom, a hydrogen donor, in the eighth position of NIC and oxygen, a hydrogen acceptor, in the seventh position of DF displayed a lower atomic fluctuation than others. This indicated the formation of a stable hydrogen bond between both molecules. The hydrogen bond analysis indicated the presence of hydrogen bonds between the aforementioned atoms for 81% of the total simulation time (Figure 1).

Characterization of the DF−NIC Cocrystal by Fourier Transform Infrared (FTIR). FTIR spectroscopy is helpful in identifying the characteristics of vibrational modes of a molecule resulting from changes in the physical state of samples, such as differences in hydrogen bonding and molecular conformations. It has been a common and reliable tool for characterizing cocrystallization.[24] In Figure 2 FTIR spectra, we have found prominent vibrational peaks in DF and NIC at 1708, 1680 cm^{-1}, split 3023, and 3114 cm^{-1}, but a red shift was found in the cocrystal leading to peaks at 1685, 3004, and 3068 cm^{-1}. The observed red shift in the stretching modes of carbonyl, hydroxyl, and amine functional groups of DF and NIC indicated the presence of hydrogen bonding interactions

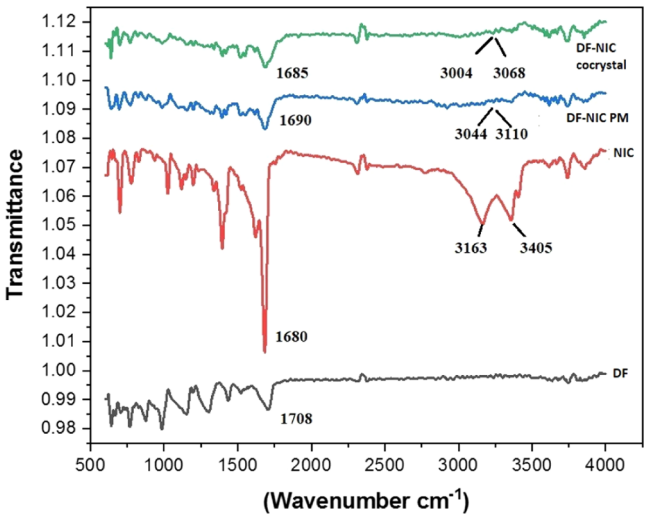

Figure 2. FTIR spectra of DF, NIC, DF−NIC physical mixture, and DF−NIC cocrystal.

as well as the formation of cocrystals. Based on the changes in the frequency of the functional groups obtained in the FTIR of the cocrystal as compared to the individual reactants and their physical mixture, we ascertained the formation of novel solid forms. Moreover, interactions between the reactants in a physical mixture (PM) can be seen leading to a red shift in the FTIR spectra due to weak forces like hydrogen bonding, among the functional groups of DF and NIC due to their physical contact while trituration during the preparation of PM. There are reports of cocrystals prepared by using NIC and their characterization by FTIR.[25]

Characterization of the DF−NIC Cocrystal by TGA. The thermal stability of a cocrystal is characterized by onset temperature (T_{onset}). Onset temperature denotes the temperature at which the weight loss begins; it can be obtained from the intersection of the baseline weight and the tangent of the weight dependence on the temperature curve as decomposition occurs.[26] As shown in Figure 3, a single-stage thermogram was obtained, and T_{onset} for pure DF, NIC,

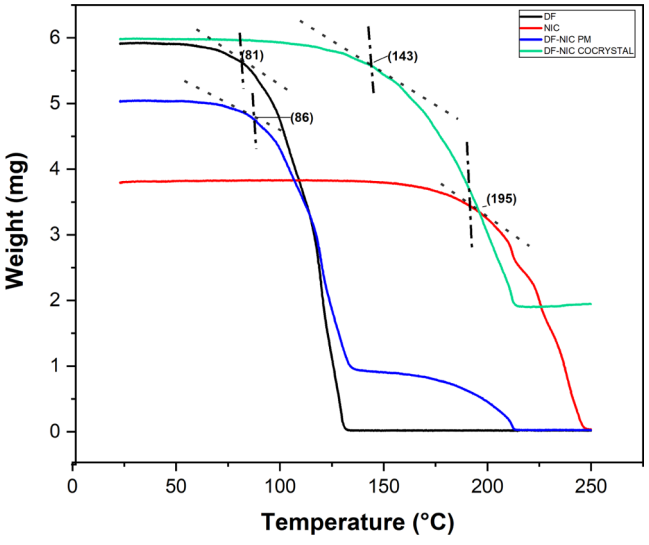

Figure 3. TGA thermogram of DF, NIC, DF−NIC PM, and DF−NIC cocrystal.

https://doi.org/10.1021/acsomega.3c02463
ACS Omega 2023, 8, 26218−26230

DF−NIC physical mixture (PM), and DF−NIC cocrystals was 81, 195, 86, and 143 °C respectively. Moreover, we have observed that DF, NIC, and DF−NIC PM have entirely decomposed up to 250 °C temperature, whereas DF has not decomposed completely by this temperature, signifying stability. The cocrystal has provided sufficient thermal stability to DF as T_{onset} has enhanced significantly in the case of the cocrystal, ensuring the chemical and thermal stability of the cocrystal.[27] There are different cocrystals reported which have provided chemical as well as thermal stability to the API or to the molecule of interest.[27,28]

Characterization of the DF−NIC Cocrystal by DSC. Melting point is one of the essential physical properties of solids, which is used to evaluate the purity of the product in which sharp melts signify purity and narrow ranges indicate the presence of impurities. A high melting point demonstrates the thermodynamical stability of the new materials, and the thermal stability of an API can be tailored by judicious selection of the coformers. Regardless of the methods used to prepare cocrystals, we have found many reports witnessing the application of differential scanning calorimetry (DSC) for a simple and rapid method to screen cocrystals.[29] In the case of the DF−NIC cocrystal, as shown in Figure 4, a single sharp

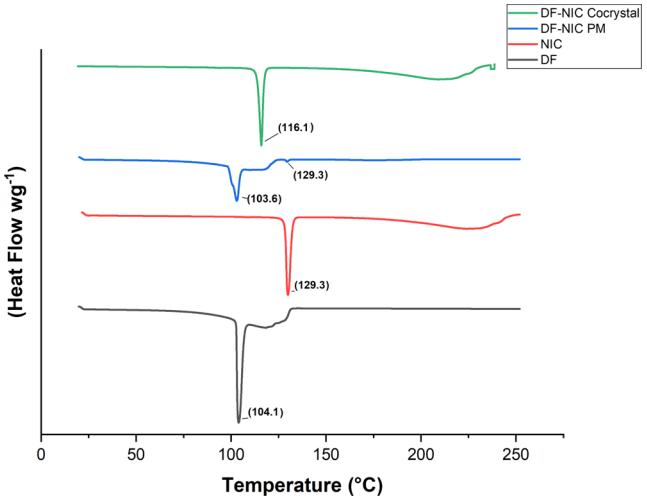

Figure 4. DSC thermogram of DF, NIC, their physical mixture, and DF−NIC cocrystal.

peak was obtained at 116 °C, but its physical mixture gave endothermic peaks at 103.6 °C and an elongated broad peak with a sharp emergent peak at 129.3 °C showing DF and NIC, respectively. However, the extension of the peak thus appearing in the cocrystal shows the interaction between them due to the new bond, indicating the formation of cocrystals. Cocrystals with the help of NIC as a coformer with single endothermic peaks have been previously reported.[30,31] Another reported cocrystal of dimethyl fumarate:gentisic acid has shown to provide stability to DF by increasing its melting point to 116.5 °C, which is significantly higher than the melting point of crystalline DF and gentisic acid (206 °C).[32]

Characterization of the DF−NIC Cocrystal Using PXRD. PXRD is considered a fingerprint characterization method for cocrystals. PXRD spectra with unique 2θ values obtained after cocrystallization, different from the reactants, indicate a new crystal solid phase.[33] In the DF−NIC cocrystal, as shown in Figure 5, new peaks that appeared at 2θ 13.2, 16.8,

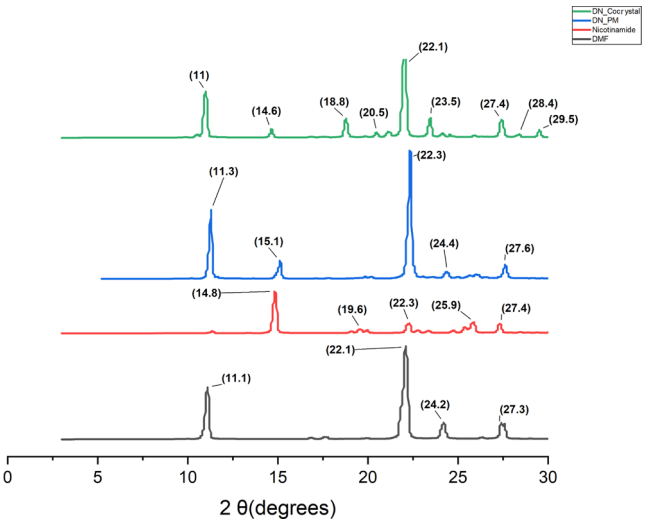

Figure 5. PXRD pattern of the DF−NIC cocrystal.

and 29.3° peak heights were altered at 2θ 18.8, 20.5, 23. 5, 28.4, and 29.5°. In another reported cocrystal of DF with gentisic acid, distinct °2θ patterns were obtained in the PXRD spectra signifying a new crystal solid phase.[32]

Effect of Cocrystallization on the Sublimation Behavior of DF. We kept DF, DF−NIC physical mixture, and DF−NIC cocrystals at 60 °C, 75% relative humidity (RH) maintained in an incubator for 20 days. With reference to Figure 6 shown below, statistical analysis using two-way

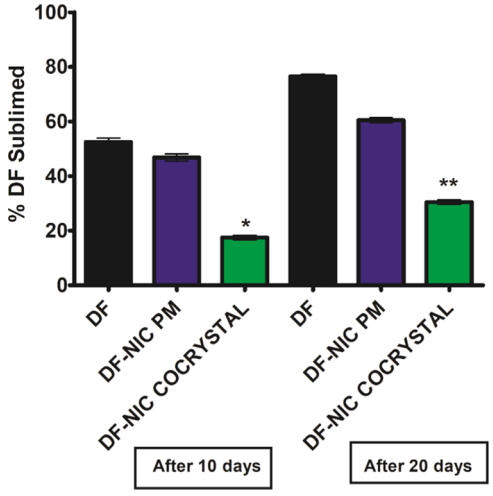

Figure 6. Sublimation of DF, its physical mixture, and its cocrystal over 20 days. Data are presented as the mean ± standard error mean (SEM), and error bars represent the SEM (n = 3). *p < 0.05 compared to DF at day 10 and **p < 0.05 compared to DF at day 20 [two-way ANOVA, followed by the Bonferroni post-hoc test].

analysis of variance (ANOVA) revealed a significant difference in % sublimed drug among the groups [F (1, 12) = 378.8, p < 0.05] and day [F (2, 12) = 778.3 p < 0.05] and an interaction between the groups and days [F (2, 12) = 16.84; P < 0.05]. The post-hoc test revealed that cocrystallization decreased the sublimation of DF significantly, as we can interpret from the result that the percentage sublimation of DF was 52.5% as compared to the cocrystals 24% for DF−NIC after day 10. We have found that after day 20, DF had sublimed by 76.5%

https://doi.org/10.1021/acsomega.3c02463
ACS Omega 2023, 8, 26218−26230

compared to the cocrystals, which had sublimed by 30.5% for DF−NIC, providing 2.5-fold protection against sublimation. Cocrystallization has been shown to provide thermal stability through hydrogen bond interactions.[34] Therefore, the DF−NIC cocrystal can prevent the sublimation of neat DF during manufacturing and storage and increase its long-term stability, thus making the drug development economic and sustainable. There are other drugs also which are prone to loss due to sublimation, like salicylic acid, in which there is significant loss from the site of application.[35] However, cocrystals have been prepared to prevent the loss due to sublimation by shielding the API.[36]

Effect of Cocrystallization on the Dissolution Profile. The dissolution profiles of DF and DF−NIC cocrystals were checked to quantify the rate of release of DF as well as to check whether cocrystal formation has led to any change in the release profile, as shown in Figure 7. Two-way ANOVA

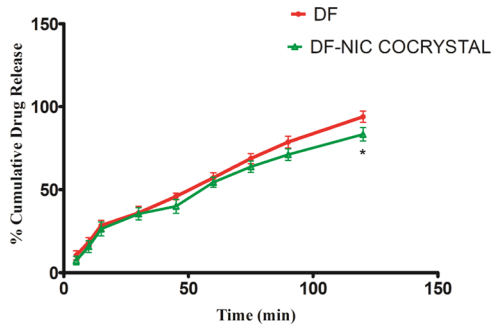

Figure 7. Percentage cumulative drug release with time for DF and its cocrystal. Data are presented as the mean ± SEM, and error bars represent the SEM (n = 3) *p < 0.05 compared to DF % cumulative release at 120 min [two-way ANOVA, followed by the Bonferroni post-hoc test].

revealed a significant difference in percent cumulative drug release among groups [F (1, 36) = 23.96, p <0.05], time [F (8, 36) = 388.1, p < 0.05] and a significant interaction between groups and time [F (8, 36) = 1.30, p < 0.05]. The post-hoc test showed that there was a significant decrease percent cumulative drug release at the 120th min only. This can be explained on the basis that cocrystals alter the solubility and rate of dissolution of the API based on its interaction with its coformers, including hydrogen bonding, solvent−solute interactions, and ionization potential.[37]

Pharmacokinetics of DF and the DF−NIC Cocrystal. The retention time for MMF was found to be 1.95 ± 0.23 min (Supporting File). As shown in Figure 8, two-way ANOVA showed no significant difference in the plasma concentration of MMF among groups [F (1, 28) = 2.196, p > 0.05], time [F (6, 28) = 58.35, p > 0.05] and a significant interaction between groups and time [F (6, 28) = 0.693, p > 0.05]. The post-hoc test showed no significant difference in the plasma concentration of MMF at any time point between DF and the DF−NIC cocrystal. It signifies no effect of cocrystallization on the absorption, distribution, metabolism, and excretion (ADME) of DF. Moreover, a correlation in *in vitro* dissolution and *in vivo* pharmacokinetics is expected and has obtained concurrence between the % cumulative release rate of the drug and pharmacokinetic parameters of DF−NIC.

Table 1, showing statistical analysis using an unpaired t-test, revealed no significant difference in the pharmacokinetic

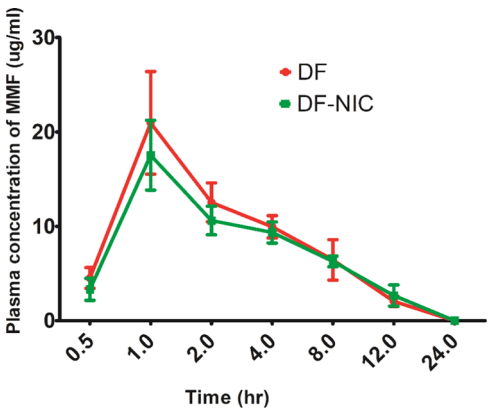

Figure 8. Plasma concentration of MMF over 24 h for DF and DF−NIC cocrystal. Data are presented as the mean ± SEM, and error bars represent the SEM (n = 3) [two-way ANOVA, followed by the Bonferroni post-hoc test].

Table 1. Pharmacokinetic Parameters of DF and DF−NIC[a]

	DF	DF−NIC
C_{max} (μg/mL)	20.954 ± 3.145	17.530 ± 2.134
T_{max} (h)	1.000 ± 0.000	1.000 ± 0.000
$T_{1/2}$ (h)	3.483 ± 0.294	4.586 ± 0.495
MRT (h)	5.676 ± 0.346	7.218 ± 0.735
AUC (0-T) (μg*hr/mL)	106.500 ± 1.320	108.900 ± 1.030

[a]Data are presented as the mean ± SEM, and error bars represent the SEM (n = 3) [unpaired t-test].

parameters (C_{max}, T_{max}, $T_{1/2}$, MRT, and AUC) of DF and DF−NIC after oral administration.

Cell Viability Assay. We have chosen PBMC as it is well known that PBMC is the target cell on which DF is known to act.[38] With reference to Figure 9 shown below, statistical

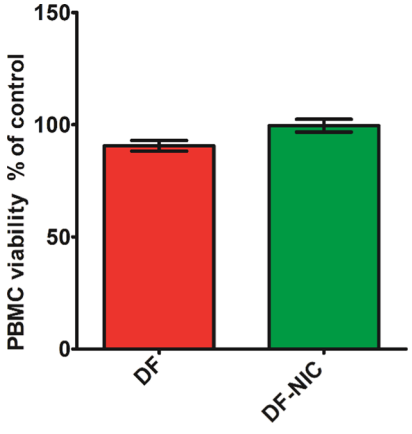

Figure 9. PBMC viability in terms of % control. Data are presented as the mean ± SEM, and error bars represent the SEM (n = 3) [unpaired t-test].

analysis using unpaired t-test revealed no significant difference in PBMC viability [F (2, 6) = 2.006, p > 0.05]. The post-hoc test revealed no significant change in the viability of the PBMC cells in the DF and DF−NIC cocrystal treatment group when compared to the vehicle control group. Thus, DF and its cocrystal can be considered as noncytotoxic and safe. Cocrystals have been shown to be noncytotoxic, as reported previously, thereby ensuring the safety of the formulation.[39]

https://doi.org/10.1021/acsomega.3c02463
ACS Omega 2023, 8, 26218−26230

Effect of the DF−NIC Cocrystal on Oxidative Stress. With reference to Figure 10 shown below, statistical analysis

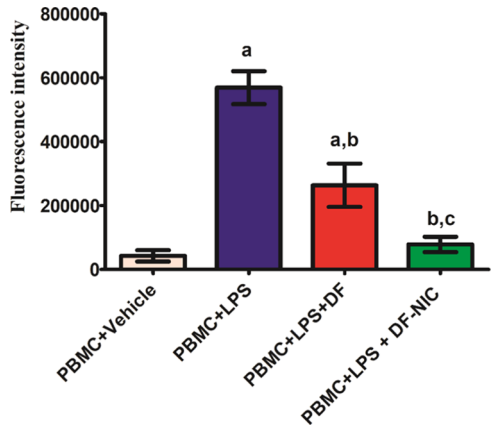

Figure 10. ROS activity on treatment with DF and DF−NIC cocrystal after LPS induction in PBMC. Data are presented as the mean ± SEM, and error bars represent the SEM (n = 4). [a]$p < 0.05$ compared to PBMC + vehicle, [b]$p < 0.05$ compared to PBMC + LPS, [c]$p < 0.05$ compared to PBMC + LPS + DF [one-way ANOVA, followed by the Newman−Keuls test].

using one-way ANOVA revealed a significant reduction in ROS [F (3, 12) = 28.27, $p < 0.05$]. The post-hoc test revealed significant fluorescence intensity in PBMC + LPS and PBMC + LPS + DF when compared to the PBMC + vehicle group. Moreover, there was no statistical difference in the fluorescence intensity between the PBMC + vehicle group and the PBMC + LPS + DF - NIC group. DF is a known potent activator of Nrf2, leading to its antioxidant activity,[40] and NIC possesses antioxidant effects by neutralizing reactive species and preventing lipid and protein oxidation.[41]

Effect of Cocrystals on IL-6 Activity. Regarding Figure 11 shown below, statistical analysis using one-way ANOVA revealed a significant difference in IL-6 release [F (3, 8) = 114.5, $p < 0.05$]. The post-hoc test showed a significant increase in IL-6 concentration in PBMC + LPS and PBMC +

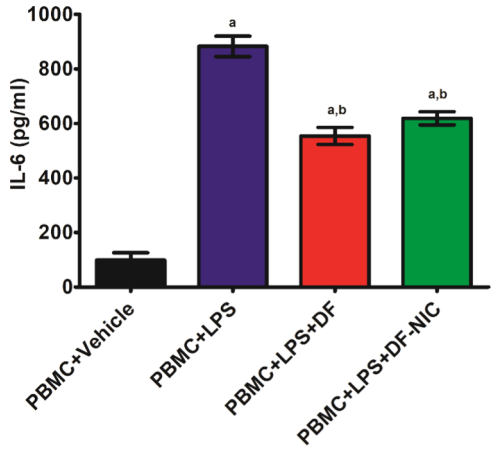

Figure 11. IL-6 activity on treatment with DF and DF−NIC after LPS induction in PBMC. Data are presented as the mean ± SEM, and error bars represent the SEM (n = 3) [a]$p < 0.05$ compared to PBMC + vehicle, [b]$p < 0.05$ compared to PBMC + LPS, [c]$p < 0.05$ compared to PBMC + LPS + DF [one-way ANOVA, followed by the Newman−Keuls test].

LPS + DF, and PBMC + LPS + DF - NIC when compared to the PBMC + vehicle group. Moreover, there was no statistical difference in the fluorescence intensity between the PBMC + LPS + DF group and the PBMC + LPS + DF−NIC group. LPS increases the expression of LPS receptors, thereby augmenting the release of IL-6 in PBMC.[42] DF and NIC inhibit inflammation by suppressing IL-6 biosynthesis, thus justifying the obtained results.[43]

Effect of Cocrystals on TNF-α Activity. Regarding Figure 12 shown below, statistical analysis using one-way ANOVA

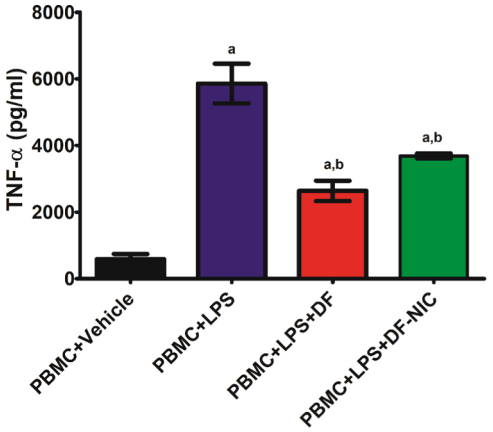

Figure 12. TNF-α activity on treatment with DF and DF−NIC cocrystal after LPS induction in PBMC. Data are presented as the mean ± SEM, and error bars represent the SEM (n = 3) [a]$p < 0.05$ compared to PBMC + vehicle, [b]$p < 0.05$ compared to PBMC + LPS [one-way ANOVA, followed by the Newman−Keuls test].

revealed a significant difference in TNF-α expression [F (3, 8) = 40.07, $p < 0.05$]. The post-hoc test revealed a significant increase in TNF-α concentration in PBMC + LPS, PBMC + LPS + DF, and PBMC + LPS + DF + NIC when compared to the PBMC + vehicle group. Moreover, there was no statistical difference in the fluorescence intensity between the PBMC + LPS + DF group and the PBMC + LPS + DF−NIC group. LPS increases inflammation by enhancing the expression of TNF-α in PBMC.[42] In previous studies, DF and NIC have been shown to possess anti-inflammatory activity by suppressing the expression of TNF-α; an analogy in the results can be seen in this study as well.[43]

Effect of the DF Cocrystal on Acute Gastric Ulcers in Rats. With reference to Figure 13 shown below, statistical analysis using one-way ANOVA revealed a significant difference in the ulcer area [F (2, 9) = 38.27, $p < 0.05$]. The post-hoc test revealed a significant ulcerated area in DF and DF−NIC cocrystal treatment groups when compared to the control group. Statistically, the DF group has a significantly more ulcerated area when compared to the DF−NIC cocrystal. Moreover, we have not evaluated the *in vitro* and *in vivo* effects of individual NIC and DF−NIC physical mixtures because our main objective was to characterize the physical and biological profile of the cocrystal. However, individual evaluation of NIC and PM would have given clear information about the role of the conformer in the cocrystal. DF has dose-dependently been shown to cause ulcers, mucosal damage, and necrosis in rat and monkey models.[4] NIC protects the GIT by preventing protein and lipid peroxidation and protecting the gastric mucus layer.[15,41]

https://doi.org/10.1021/acsomega.3c02463
ACS Omega 2023, 8, 26218−26230

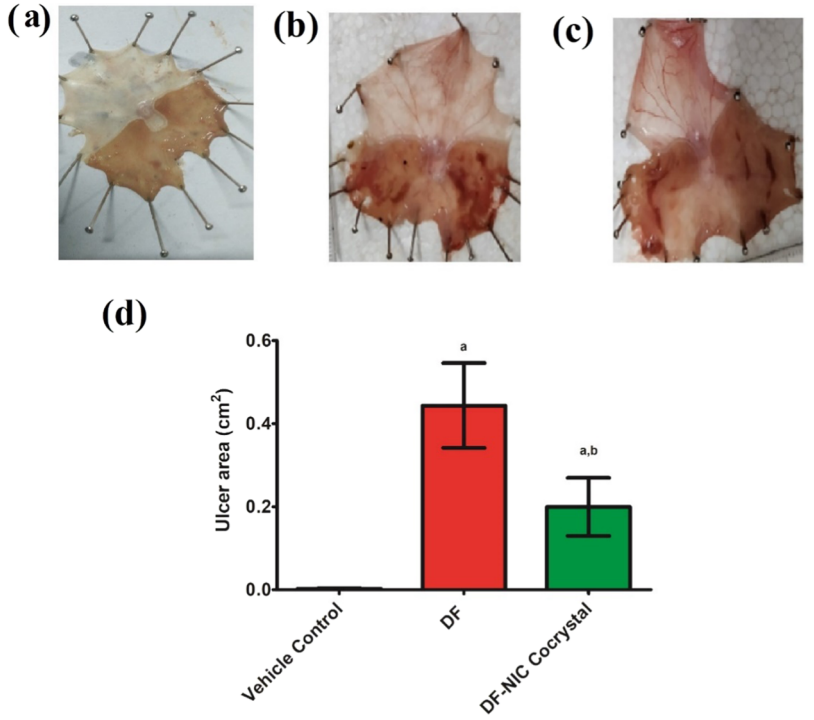

Figure 13. Ulcer area (cm^2): (a) vehicle control group, (b) treatment with DF, (c) DF−NIC cocrystal, and (d) ulcer area statistics. Data are presented as the mean ± SEM, and error bars represent the SEM ($n = 3$) $^{a}p < 0.05$ compared to the vehicle control, $^{b}p < 0.05$ compared to DF [one-way ANOVA followed by the Newman−Keuls test].

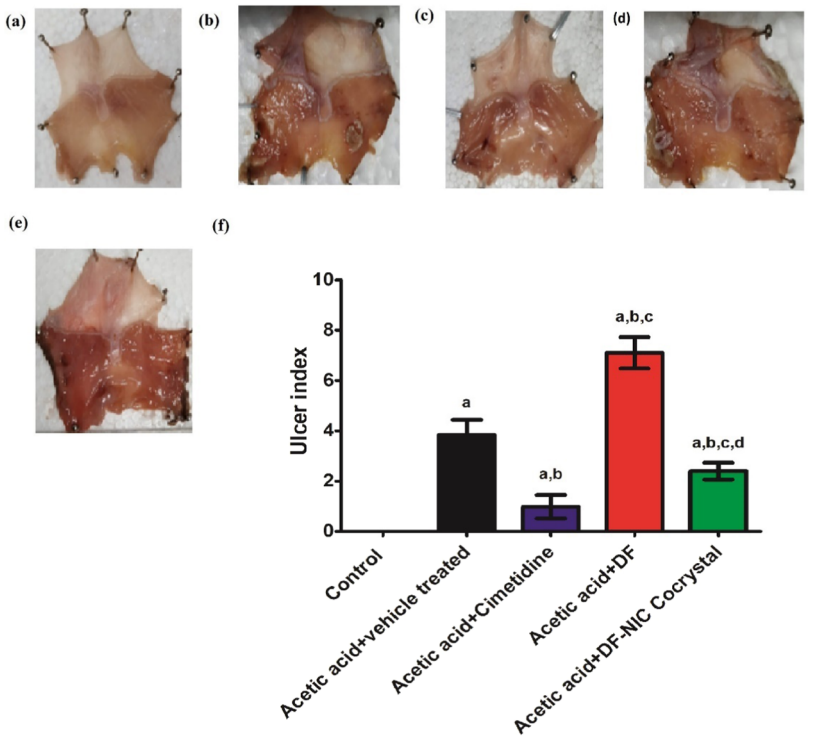

Figure 14. Ulcer index: (a) control group, (b) acetic acid + vehicle group, (c) acetic acid + cimetidine group, (d) acetic acid + DF, (e) acetic acid + DF−NIC cocrystal, and (f) ulcer index statistics. Data are presented as the mean ± SEM, and error bars represent the SEM ($n = 5$). $^{a}p < 0.05$ compared to the control, $^{b}p < 0.05$ compared to the acetic acid + vehicle control, $^{c}p < 0.05$ compared to acetic acid + cimetidine, $^{d}p < 0.05$ compared to acetic acid + DF [one-way ANOVA, followed by the Newman−Keuls test].

Effect of the DF Cocrystal on Acetic Acid-Induced Chronic Gastric Ulcers. With reference to Figure 14 shown below, statistical analysis using one-way ANOVA revealed significant differences in the ulcer index [$F(4, 10) = 107.5$, $p < 0.05$]. The post-hoc test revealed a significant ulcer index in the acetic acid + vehicle treatment group, acetic acid + DF,

https://doi.org/10.1021/acsomega.3c02463
ACS Omega 2023, 8, 26218−26230

acetic acid + cimetidine, and acetic acid + DF−NIC cocrystal treatment group when compared to the control group. Statistically, the DF group has significantly more ulcerated area when compared to the DF−NIC cocrystal. DF has an ulcerogenic effect, as shown in the previous study,[4] which can justify the high ulcer index in the group, and NIC has a comparative gastroprotective activity, which has imparted a low gastric index in the DF−NIC cocrystal group.[15]

Effect of the DF Cocrystal on Gastric Malondialdehyde (MDA) Activity. With reference to Figure 15 shown below, statistical analysis using one-way ANOVA revealed significant differences in lipid peroxidation [F (4, 20) = 28.86, $p < 0.05$]. The post-hoc test revealed a significant increase in lipid peroxidation in the acetic acid + vehicle and acetic acid + DF treatment groups compared to the control group. However, there is no significant difference between the control, acetic acid + DF−NIC, and acetic acid + cimetidine groups. Moreover, the acetic acid + vehicle treatment group and acetic acid + DF group have significantly more lipid peroxidation when compared to the DF−NIC cocrystal and acetic acid+cimetidine group. Gastric ulcers are associated with elevated MDA levels due to reactive oxygen species, which may, in turn, promote lipid peroxidation.[44] This is probably due to the ability of NIC to inhibit the initiation step of lipid peroxidation in the gastric tissue.[41]

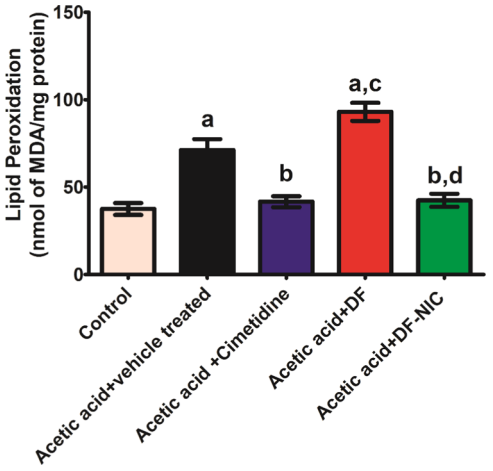

Figure 15. Lipid peroxidation in the gastric tissue on treatment with DF and DF−NIC after acetic acid-induced ulcers. Data are presented as the mean ± SEM, and error bars represent the SEM (n = 5). $^{a}p < 0.05$ compared to the control, $^{b}p < 0.05$ compared to the acetic acid + vehicle control, $^{c}p < 0.05$ compared to acetic acid + cimetidine, $^{d}p < 0.05$ compared to acetic acid + DF [one-way ANOVA, followed by the Newman−Keuls test].

Effect of the DF Cocrystal on the Gastric Total Nitrite Level. With reference to Figure 16 shown below, statistical analysis using one-way ANOVA revealed significant differences in the total nitrite level [F (4, 20) = 26.09, $p < 0.05$]. The post-hoc test revealed a significant decrease in the total nitrite level in acetic acid + vehicle and acetic acid + DF treatment groups compared to the control group, acetic acid + DF−NIC group, and acetic acid + cimetidine group. However, there is a significantly reduced nitrite in the acetic acid + DF group as compared to the acetic acid + vehicle-treated group. Gastric total nitrite and nitrate have gastroprotective effects,[45] and its reduced levels are found in the acetic acid-induced gastric ulcer model.[44] DF is known to cause gastrointestinal (GI) adverse

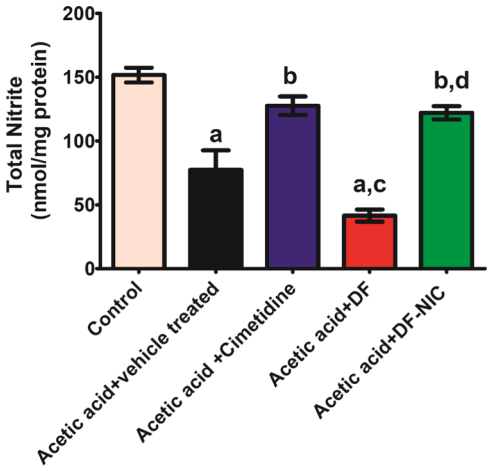

Figure 16. Total nitrite in the gastric tissue on treatment with DF and DF−NIC after acetic acid-induced ulcers. Data are presented as the mean ± SEM, and error bars represent the SEM (n = 5) $^{a}p < 0.05$ compared to the control, $^{b}p < 0.05$ compared to the acetic acid + vehicle control, $^{c}p < 0.05$ compared to acetic acid + cimetidine, $^{d}p < 0.05$ compared to acetic acid + DF [one-way ANOVA, followed by the Newman−Keuls test].

effects.[4] NIC illicits gastroprotective effects[15] by increasing nitric oxide, which attributes to the availability of an important cofactor called NADPH, crucially involved in the biogenesis of nitric oxide from arginine amino acid.[46]

CONCLUSIONS

In this study, we have prepared novel cocrystals of DF with NIC as a coformer based on their predictability to participate in hydrogen bonding and GRAS (generally regarded as safe). Cocrystals have been formulated by using the solvent evaporation method and characterized by using spectral techniques of FTIR and diffractometry techniques of PXRD. The thermal evaluation has been done using TGA and DSC. Dissolution and pharmacokinetic studies compare the release profile of DF with its cocrystal in *in vitro* and *in vivo* systems, respectively. The cytotoxic and biological activity of DF has been compared with that of the cocrystals. For the very first time, DF cocrystals have been made to troubleshoot its sublimation problem and to counterbalance its adverse effects, which will ultimately lead to enhanced processability of the API during its formulation and patient safety and compliance.

MATERIALS AND METHODS

***In Silico* Experiment.** *Molecular Docking.* The structures of NIC and dimethyl fumarate were sketched with the help of ChemDraw 15. Further, they were converted into three-dimensional (3D) structures through energy minimization using the MMFF94s force field. These mol2 files were converted to pdbqt using Autodock tools 1.5.6. Autogrid-4.0 was used to calculate grid maps of interaction energies among the various types of atoms present (A, C, HD, NA, N, OA, S). The grid box size was set to 40 × 40 × 40 with a grid spacing of 0.375 Å. The grid centered around coordinates (x, y, and z) 0.423, 0.316, and 0.0. The docking was performed by Autodock-4.2.6 using the Lamarckian Genetic Algorithm with 10 runs, 150 population size, 2,500,000 maximum number of energy evaluations, and 27,000 maximum number of generations.[47] The docked structure was visualized by using Discovery Studio 2020.[48]

https://doi.org/10.1021/acsomega.3c02463
ACS Omega 2023, 8, 26218−26230

Molecular Dynamics. The obtained poses of ligands were parameterized through an *antechamber* toolkit using a general AMBER force field (GAFF2) and the Austin model with bond and charge correction (AM-BCC1) atomic partial charges. The topologies and coordinates for the complex of DF and NIC were built using the *tleap* module of AMBER 20. It was hydrated with TIP3P water molecules in a cubic box with a cutoff distance of 12 Å and neutralized by adding Na+ and Cl^- ions. The systems were subjected to energy minimization, heating, density equilibration, and equilibration under periodic boundary conditions.[49] The final 5 ns molecular dynamics (MD) was carried out at 310.15 K as an NPT ensemble. Further, the post-MD processing was carried out using *cpptraj*.[50]

Experimental Animals. Inbred male adult Sprague−Dawley rats weighing between 180 and 220 g were procured from the Central Animal House, Institute of Medical Science (IMS-BHU). The experiments were performed by adopting guidelines (NIH publication number 85−23, revised 2015) and approved by the Institutional Animal Ethical Committee, Banaras Hindu University (BHU; Dean/2019/CAEC/1649). Animals were acclimatized in the experimental lab before using them for experiments for 1 week of acclimatization under standard laboratory conditions (22 ± 2 °C, 12 h light/dark cycle, and relative humidity of 50 ± 5%).

Materials. DF was obtained from Disto Pharmaceuticals (Hyderabad, India) as a gift sample, NIC and sodium chloride were purchased from Merck, MTT was obtained from SRL chemicals, Hisep was obtained from Himedia (India), LPS (*E. coli*, L3129), MMF, dichlorofluorescein diacetate, trypan blue, and antibiotics were obtained from Sigma-Aldrich, RPMI-1640 and FBS were obtained from Lonza, and TNF-α and IL-6 ELISA kits were purchased from Krishgen Biosystems (Mumbai, India). Ultrapure water was prepared using a Milli-Q Ultrapure purification system (Millipore). Countess cell counting chamber slides were purchased from Thermo Fisher. All other chemicals and reagents of high-performance liquid chromatography (HPLC) and analytical grade were procured from local suppliers.

Method of Preparation of the Cocrystal. The cocrystal was formulated by the solvent evaporation method.[51] It is a commonly used method for the preparation of cocrystals. This technique is based on the solubility profile of the API and the coformer. The method requires the drug substance and the coformer to get dissolved in a common solvent, which is allowed to get evaporated slowly over a period of time. The technique works on the principle of the formulation of hydrogen bonds in a favorable drug substance and a complementary coformer.[17] For making the DF−NIC cocrystal, DF and NIC were taken in a 1:1 molar ratio and dissolved separately in excess of ethanol. Both were mixed to get a clear homogenous solution. The solution was passed through a 0.22 μm membrane filter to avoid any undissolved particles. It was kept in a glass container fully covered with aluminum foil with small holes to facilitate solvent evaporation. It was kept undisturbed in an incubator set at 40 °C for slow solvent evaporation to get fine cocrystals. The evaporation rate controls the process of crystallization; the more time is provided for evaporation, the larger the crystals are obtained. The resulting product was dried in an oven at 80 °C overnight to remove the residual solvent and gently ground to a fine powder for further analysis.

Preparation of the Physical Mixture. The physical mixture (PM) was prepared by taking DF and NIC in similar ratios and triturating them gently in a mortar and pestle. This PM was used as a control to compare the DF−NIC cocrystal.

Characterization of Cocrystals. *Fourier Transform Infrared (FTIR) Spectroscopy.* FTIR spectral region was set from 400 to 4000 cm^{-1} obtained using a Shimadzu IR-Prestige-21 FTIR spectrometer coupled with a horizontal golden gate MKII single-reflection attenuated total reflectance (ATR) system (Specac, Kent, U.K.) equipped with ZnSe lenses after appropriate background subtraction. All of the spectral data were collected at ambient temperature. Data were collected and analyzed by the built-in software.

Powder X-ray Diffraction (PXRD). PXRD was conducted by a MiniFlex II benchtop X-ray diffractometer at 30 kV and 15 mA with a Ni-filtered Cu Kα radiation source (λ) 1.54 Å (Rigaku, The Woodlands, TX). The samples were scanned from 5 to 30° (2θ) at a scanning rate of 0.5 °C per min. The diffractograms were processed using Origin Pro.

Characterization of Cocrystals by TGA and DSC. The melting point is one of the essential physical properties of solids, which is used to determine the purity of the product. A high melting point demonstrates the thermodynamic stability of the new materials, *i.e.*, the thermal stability of an API can be increased by selecting the coformer with the higher melting point.[52] The most commonly used techniques for determining the melting point and thermal stability analysis are thermal gravimetric analysis (TGA) and differential scanning calorimetry (DSC).[53] The melting point of pharmaceutical cocrystals can be tailored by judicious selection of the coformers, which could provide thermal stability to the complimentary API.[54]

Differential Scanning Calorimetry (DSC). DSC was conducted by use of a DSC-60 Plus Shimadzu differential scanning calorimeter. Accurately weighed samples (4−7 mg) were placed in hermetically sealed aluminum pans and scanned from 25 to 250 °C at 10 °C/min under a nitrogen purge. The DSC calibration was done using a single-point method with the extrapolated onset of the melting point of 0.275 mg of a sample of indium.

Thermogravimetric Analysis (TGA). The decomposition temperature for each substance was determined using a Shimadzu Corporation TGA-50 Thermogravimetric analyzer. Approximately 4−7 mg amount of the sample was heated from 25 to 250 °C at a 10 °C/min rate. A purge of dry nitrogen (flow rate sample, 60 mL/min; flow rate balance, 40 mL/min) was maintained through the sample chamber during all of the experiments to keep an inert environment and to avoid any prevent oxidation of samples.

Evaluation of the Cocrystal to Check Sublimation Behavior. The sublimation behavior of DF and the cocrystal were evaluated by following the method of physical stability with some modifications.[30] A known amount of DF and the DF−NIC cocrystal and their physical mixtures was prepared by gentle trituration of DF and the coformer in the same ratios, which have been taken for the cocrystal in a glass vial. The mouth of the glass vials was covered with perforated aluminum foil. These glass vials were maintained in an incubator at 60 °C, 75% RH for a period of 20 days. As approx. 80% of DF sublimed by the 20th day, it was kept in this condition for not more than 20 days. Relative humidity was maintained using a saturated solution of sodium chloride kept in a beaker in the same incubator.[55] % DF sublimed was analyzed after 10 and 20 days from the day it was kept in the incubator.

https://doi.org/10.1021/acsomega.3c02463
ACS Omega 2023, 8, 26218−26230

Dissolution Rate Analysis. Dissolution was carried out following the method as per FDA (www.accessdata.fda.gov/scripts/cder/dissolution). 100 mg each of DF and various cocrystals were filled into empty capsule shells and taken into 500 mL phosphate buffer (pH 6.8) at the beginning of the dissolution experiments. The mixtures in the dissolution tester were stirred at 37 °C and 100 rpm. At each time interval, 5 mL of the solution was withdrawn from the instrument and replaced by an equal volume of buffer to maintain the sink condition in the experiment. The solution was filtered by a 0.22 μm nylon filter before measuring DF concentration and was analyzed by HPLC.

HPLC Analysis. DF quantification was performed by HPLC using Agilent technologies HPLC, Infinity 1260 II equipped with a degasser, a quaternary pump, and an autosampler. (20A3). The system includes a diode array detector and a computer running Agilent openLAB CDS control panel help software for data acquisition and processing. Chromatographic separation was performed at 25 ± 1 °C by using a C8 column (4.6 mm × 250 mm, 5 μm) preceded by a guard column of the same packing material. The mobile phase used consisted of acetonitrile and water (80:20). The flow rate was set at 1.0 mL/min, and the total sample acquisition time was 10 min. Based on previous studies, the ultraviolet (UV) detector was set at 220 nm, and the injection volume was set at 10 μL. For MMF quantification, the solvent system was methanol/potassium phosphate buffer supplemented with 5 mM tetrabutylammonium dihydrogen phosphate 20:80 (v/v) with a detector set at 215 nm.[56]

***In Vitro* Evaluation of the Biological Activity of Cocrystals.** *Isolation of Peripheral Blood Mononuclear Cells (PBMCs).* Blood was collected from a Sprague−Dawley rat through the terminal method (cardiac puncture) and taken into EDTA vacutainer tubes. It was diluted with an equal volume of phosphate-buffered saline (PBS). Mononuclear cells were separated from peripheral blood samples according to the method described with modifications.[21,42] Briefly, 3 mL of the blood mixture was gently layered over 2 mL of Hisep (Ficoll) solution and centrifuged at 1000*g* for 25 min. The white band of mononuclear cells was collected and washed thrice with RPMI-1640 culture medium by centrifugation at 1000*g* for 5 min. PBMCs were resuspended in complete RPMI-1640 culture medium (RPMI-1640 medium containing 25 mM HEPES), 2 mM L-glutamine, 10% heat-inactivated fetal calf serum, penicillin (100 U/mL), and streptomycin (100 μg/mL) and adjusted to 2 × 10^6 cells/mL.

PBMC Counting via the Trypan Blue Exclusion (TBE) Assay. Cell count was done using the trypan blue dye exclusion technique with the help of a Countess II automated cell counter using the trypan blue exclusion (TBE) method.[57] After isolating the PBMC, 10 μL aliquots of the sample were mixed with 10 μL of trypan blue (0.4%) (Invitrogen, Italy). It was put into Countess cell counting chamber slides, and the count was made by a Countess automated cell counter (Invitrogen, Italy).

Cytotoxicity Assay. The MTT assay was performed to evaluate the cytotoxicity of DF-NIC cocrystal in comparison with pure DF.[58] The MTT dye, *via* reductive cleavage of its tetrazolium ring, is converted to purple water-insoluble formazan in the presence of mitochondrial succinate dehydrogenase in living cells. Thus, the assay signifies the ability of metabolically active cells to reduce MTT to formazan. In other words, the amount of formazan produced serves as a direct indicator of the number of viable cells in the sample. 100 μL of PBMC aliquots were taken in RPMI-1640 containing 20% FBS taken in a microculture well. 20 and 10 μg/mL cocrystal and DF were added into the microculture well. Blank and vehicle control groups were taken accordingly. The culture plate was incubated for 12 h at 37 °C in 5% CO_2 conditions in the incubator chamber. 10 μL of MTT (5 mg/mL) was added into the microculture wells and again kept for 2 h at 37 °C and 5% CO_2 conditions in the incubator. 100 μL of DMSO was added to it and kept again for 2 h. Absorbance was taken at 570 nm.

Cytokine Analysis. Evaluation of the cocrystal for anti-inflammatory activity was done against LPS-induced PBMC.[59] PBMC (2 × 10^6 cells/mL) was taken in 100 μL aliquot and incubated with and without LPS (10 μg/mL) in 100 μL of RPMI containing 20% FCS for 24 h in a humidified atmosphere of 5% CO_2 at 37 °C. Later, it was washed twice with PBS and incubated with DF and its cocrystal containing an equivalent of 10 μg/mL DF for 12 h. It was washed twice again with PBS. Further, it was incubated for 2 h with RPMI containing 20% FCS. It was centrifuged at 1500 × *g* for 5 min to obtain a clear supernatant. The supernatant was cryopreserved for further cytokine activity. IL-6 and TNF-α levels in the supernatant were determined using commercial enzyme-linked immunosorbent assay (ELISA) kits.

Measurement of Intracellular ROS (iROS). Intracellular ROS was detected using DCFH-DA, which crosses cell membranes and gets hydrolyzed into nonfluorescent DCFH by intracellular esterases. However, DCFH is oxidized to highly fluorescent dichlorofluorescein (DCF) in the presence of ROS, which is readily detectable by fluorescence-based instruments like FACS or a spectrofluorometer. Intracellular ROS were measured in the PBMC treated with LPS, and further, DF and its cocrystal were evaluated against LPS using the following method.[60] PBMC were counted for total viable cells by the trypan blue exclusion assay with the help of a Countess II automated cell counter. 100 μL aliquot (2 × 10^5 cells) was incubated with LPS (10 μg/mL) in 100 μL of RPMI containing 20% FCS for 24 h in a humidified atmosphere of 5% CO_2 at 37 °C. Later, it was washed twice with PBS and incubated with 10 μg/mL DF and the cocrystal containing an equivalent of 10 μg/mL DF for 12 h. It was washed twice again with PBS. iROS were labeled by incubating cells in 100 μL of 20 mM dichlorofluorescein diacetate (DCFH-DA) for 45 min at 37 °C temp in the dark. After incubation, fluorescence intensity was monitored by using a multimode reader (λ_{ex}: 490 nm; λ_{em}: 515 nm).

Pharmacokinetic Study. Pharmacokinetic data of DF and its cocrystal were evaluated in healthy male Sprague−Dawley rats weighing 150−200 g, following the method in ref 61. Animals were divided into four groups including 3 animals in each group. Animals were made to fast overnight before the experiment, but water was given *ad libitum*. The animals were given an oral dose of 100 mg/kg DF and its cocrystal containing the same amount of DF. Blood samples (0.25 mL) were isolated *via* retro-orbital under ether anesthesia in the heparin-treated tube at 0.5, 1, 2, 4, 8, 12, and 24 h. Plasma was isolated from blood samples by centrifuging at 7000 rpm for 5 min at 4 °C. The isolated plasma containing the drug (DF) was extracted by precipitating it with an equal volume of acetonitrile. It was vortexed for a minute and centrifuged at 13,000 rpm for 15 min. The clear supernatant was isolated and filtered at 0.22 μm for further HPLC analysis.

https://doi.org/10.1021/acsomega.3c02463
ACS Omega 2023, 8, 26218−26230

Acute Gastric Ulcer Model of Rats. DF is known to cause GIT irritation, anal incontinence, diarrhea, dyspepsia, irritable bowel syndrome, and peptic ulcers.[62] We have developed an acute gastric ulcer model with DF, taking DF at a higher dose (400 mg/kg), which has been shown to cause gastric ulceration.

Animals were divided into three groups containing three animals in each group, namely, the vehicle control, DF group, and DF−NIC group. Animals were fasted for 16 h by placing them in a cage with a perforated base to avoid coprophagy. Water was given *ad libitum*. Acute gastric ulcers were induced by dosing the animals with DF (400 mg/kg) dispersed in 0.5% carboxymethyl cellulose (CMC) and DF−NIC cocrystal containing 400 mg/kg DF dispersed in 0.5% CMC. The vehicle group was provided with 0.5% CMC only. Dosing was done by the intragastric route using a long smooth gastric tube to avoid gastritis of the oral and oesophagal mucosal layer.

Acetic Acid-Induced Chronic Gastric Ulcers in Rats. The acetic acid model of gastric ulcers is a common method that has some resemblance to an acute, chronic gastric ulcer in humans. Chronic gastric ulcers were induced in rats by the method with slight modifications.[63] Sprague−Dawley rats were randomly assigned into five groups consisting of five animals in each group. The animals were deprived of food for 24 h but allowed free access to water before gastric ulcer induction. They were kept in a net-based perforated cage to avoid coprophagy. Briefly, animals were anesthetized with ketamine and xylazine. When anaesthetization is confirmed, a cut of an approx. 2 cm opening was made from the middle of the xiphoid process along the middle line of the abdomen. The stomach is traced, and it is gently pulled out without disturbing the other vitals. The antrum wall of the stomach was identified, and it was cleaned with a smooth cotton swab. Meanwhile, a disc of filter paper about 5 mm in diameter and specified thickness (measurement kept constant for the experiment) was dipped with the proper amount of glacial (99.5%) acetic acid. It was applied for 30 s × 2 times (one filter paper per time) to the serous layer of the antrum of the stomach. Immediately, the surface containing acetic acid was wiped away, and it was washed with PBS buffer. The rats were taken care till they recovered. These rats were fasted for one day. For the control group, rats were treated with filter paper soaked in PBS only. After 48 h of the ulcer induction, groups of animals were treated with water in the vehicle group, DF in the acetic acid + DF group, cimetidine as the standard treatment group, and DF−NIC cocrystal in the test group once daily for 7 days.[64]

Evaluation of Gross Lesions on the Gastric Mucosa. The total ulcer area was measured using the National Institute of Health (NIH) Image-J software. The ulcer index and the rate of protection of ulceration were calculated by the following formula: ulcerated pixel number/total gastric pixel amount X 100.[65]

Determination of Related Biochemical Indexes in Gastric Tissues. The stomach tissues were isolated, minced with sharp blades, and homogenized with cold PBS buffer, pH 7.2 (w/v,1: 9), and the obtained homogenate was centrifuged for 10 min at 2500 rpm to obtain the supernatant for the determination of the MDA/lipid peroxidation activity and total nitrite level. Lipid peroxidation was evaluated as the formation of thiobarbituric acid-reactive compounds, which are formed when MDA is heated with thiobarbituric acid, generating a pink color. Its absorbance was taken at 532 nm in a multimode reader (Biotek), and the results were expressed as nanomoles of MDA per gram of the gastric tissue. Total proteins were determined by the Bradford reagent. The total nitrite level was estimated by the Griess reagent in which nitrite is assayed in the sample as a reduction product of nitrate into nitrite.[66]

Statistical Analysis. All values are expressed as the mean ± standard error mean (SEM). Two-way ANOVA, followed by the Bonferroni post-hoc test, was performed to compare % sublimation at day 10 with day 20 and also to compare the % cumulative dissolution rate at different time points for DF and its cocrystal. One-way ANOVA, followed by the post-hoc Student−Newman−Keuls test, was performed for the analysis of all other biochemical parameters using Graph Pad Prism version 5 (San Diego, CA). Groups with $p < 0.05$ were considered significantly different. Various spectra were overlayed using Origin 2018. Pharmacokinetic data were analyzed using Kinetika 5.0 software.

■ ASSOCIATED CONTENT

Data Availability Statement

The datasets are available in the Supporting File.

Supporting Information

The Supporting Information is available free of charge at https://pubs.acs.org/doi/10.1021/acsomega.3c02463.

Raw data of the experiment including sublimation data, RMSD and RMSF data; hydrogen bonding data; cocrystal characterization data; dissolution and pharmacokinetics data; retention time of MMF, and biological experiment data (XLSX)

■ AUTHOR INFORMATION

Corresponding Author

Sairam Krishnamurthy − *Neurotherapeutics Laboratory, Department of Pharmaceutical Engineering & Technology, Indian Institute of Technology (Banaras Hindu University), Varanasi 221005 U.P., India*; orcid.org/0000-0003-4159-2463; Phone: +91-9935509199; Email: ksairam.phe@iitbhu.ac.in, saibliss@hotmail.com; Fax: +91-542-2368428

Authors

Qadir Alam − *Neurotherapeutics Laboratory, Department of Pharmaceutical Engineering & Technology, Indian Institute of Technology (Banaras Hindu University), Varanasi 221005 U.P., India*

Ankit Ganeshpurkar − *Pharmaceutical Chemistry Laboratory, Department of Pharmaceutical Engineering & Technology, Indian Institute of Technology (Banaras Hindu University), Varanasi 221005 U.P., India*

Sushil Kumar Singh − *Pharmaceutical Chemistry Laboratory, Department of Pharmaceutical Engineering & Technology, Indian Institute of Technology (Banaras Hindu University), Varanasi 221005 U.P., India*

Complete contact information is available at: https://pubs.acs.org/10.1021/acsomega.3c02463

Notes

The authors declare no competing financial interest.

The ethical approval was taken from Institutional Animal Ethical Committee (IAEC), Banaras HinduUniversity (BHU; Dean/2019/CAEC/1649).

■ ACKNOWLEDGMENTS

The support and the resources provided by "The PARAM Shivay Facility" under the National Supercomputing Mission, Government of India, at the Indian Institute of Technology (BHU), Varanasi, are gratefully acknowledged. The authors would also like to extend their gratitude toward Professor David A. Case, Department of Chemistry & Chemical Biology, Rutgers University, New Jersey, for granting a license for AMBER 20.

■ REFERENCES

(1) Deeks, E. D. Dimethyl fumarate: a review in relapsing-remitting MS. *Drugs* **2016**, *76*, 243−254.
(2) Kawakami, T.; Isama, K.; Matsuoka, A.; Nishimura, T. Determination of dimethyl fumarate and other fumaric and maleic acid diesters in desiccants and consumer products in Japan. *J. Health Sci.* **2011**, *57*, 236−244.
(3) Zawaneh, P.; Karki, S. B.; Kaufman, M.; Leung, C.-Y.; Dong, J.; Quan, E.; Vasudevan, K. Controlled Release Dosage Form for Once Daily Administration of Dimethyl Fumarate, 2019.
(4) McCullough, T.; Annamalai, T.; Wustrow, D.; Cundy, K. *Comparative Gastric Irritation of the Fumaric Acid Esters Dimethyl Fumarate (DMF) and XP23829 in Rat and Monkey (P01. 159)*; AAN Enterprises, 2013.
(5) Mrowietz, U.; Szepietowski, J. C.; Loewe, R.; van de Kerkhof, P.; Lamarca, R.; Ocker, W. G.; Tebbs, V. M.; Pau-Charles, I. Efficacy and safety of LAS 41008 (dimethyl fumarate) in adults with moderate-to-severe chronic plaque psoriasis: a randomized, double-blind, Fumaderm-and placebo-controlled trial (BRIDGE). *Br. J. Dermatol.* **2017**, *176*, 615−623.
(6) Landenberger, K. B.; Bolton, O.; Matzger, A. J. Two isostructural explosive cocrystals with significantly different thermodynamic stabilities. *Angew. Chem.* **2013**, *125*, 6596−6599.
(7) Khajir, S. *Preparation and Investigation on the Stability of Salt or Cocrystal forms of Valproic Acid and Carbamazepine*; Tabriz University of Medical Sciences, Faculty of Pharmacy, 2020.
(8) Machado, T. C.; Gelain, A. B.; Rosa, J.; Cardoso, S. G.; Caon, T. Cocrystallization as a novel approach to enhance the transdermal administration of meloxicam. *Eur. J. Pharm. Sci.* **2018**, *123*, 184−190.
(9) Likhitha, U.; Narayana, B.; Sarojini, B.; Lobo, A. G.; Sharma, G.; Pathania, S.; Kant, R. Do hydrogen bonding and noncovalent interactions stabilize nicotinamide-picric acid cocrystal supramolecular assembly? *J. Mol. Struct.* **2019**, *1195*, 827−838.
(10) Aakeröy, C. B.; Fasulo, M. E.; Desper, J. Cocrystal or salt: does it really matter? *Mol. Pharmaceutics* **2007**, *4*, 317−322.
(11) Cavanagh, K. L.; Maheshwari, C.; Rodríguez-Hornedo, N. Understanding the differences between cocrystal and salt aqueous solubilities. *J. Pharm. Sci.* **2018**, *107*, 113−120.
(12) Cheney, M. L.; Weyna, D. R.; Shan, N.; Hanna, M.; Wojtas, L.; Zaworotko, M. J. Coformer selection in pharmaceutical cocrystal development: a case study of a meloxicam aspirin cocrystal that exhibits enhanced solubility and pharmacokinetics. *J. Pharm. Sci.* **2011**, *100*, 2172−2181.
(13) Galetzka, C.; Rundfeldt, C.; Rupp, R.; Andersen, P. M. Pharmaceutical composition containing dimethyl fumarate for administration at a low daily dose, 2019.
(14) Lu, J.; Rohani, S. Preparation and characterization of theophylline− nicotinamide cocrystal. *Org. Process Res. Dev.* **2009**, *13*, 1269−1275.
(15) Abdallah, D. M. Nicotinamide alleviates indomethacin-induced gastric ulcers: a novel antiulcer agent. *Eur. J. Pharmacol.* **2010**, *627*, 276−280.
(16) Fucke, K.; Myz, S. A.; Shakhtshneider, T. P.; Boldyreva, E. V.; Griesser, U. J. How good are the crystallisation methods for co-crystals? A comparative study of piroxicam. *New J. Chem.* **2012**, *36*, 1969−1977.
(17) Karimi-Jafari, M.; Padrela, L.; Walker, G. M.; Croker, D. M. Creating cocrystals: a review of pharmaceutical cocrystal preparation routes and applications. *Cryst. Growth Des.* **2018**, *18*, 6370−6387.
(18) Mills, E. A.; Ogrodnik, M. A.; Plave, A.; Mao-Draayer, Y. Emerging understanding of the mechanism of action for dimethyl fumarate in the treatment of multiple sclerosis. *Front. Neurol.* **2018**, *9*, No. 5.
(19) Brück, J.; Dringen, R.; Amasuno, A.; Pau-Charles, I.; Ghoreschi, K. A review of the mechanisms of action of dimethylfumarate in the treatment of psoriasis. *Exp. Dermatol.* **2018**, *27*, 611−624.
(20) Werdenberg, D.; Joshi, R.; Wolffram, S.; Merkle, H.; Langguth, P. Presystemic metabolism and intestinal absorption of antipsoriatic fumaric acid esters. *Biopharm. Drug Dispos.* **2003**, *24*, 259−273.
(21) Moharregh-Khiabani, D.; Blank, A.; Skripuletz, T.; Miller, E.; Kotsiari, A.; Gudi, V.; Stangel, M. Effects of fumaric acids on cuprizone induced central nervous system de-and remyelination in the mouse. *PLoS One* **2010**, *5*, No. e11769.
(22) Fiedler, S. E.; George, J. D.; Love, H. N.; Kim, E.; Spain, R.; Bourdette, D.; Salinthone, S. Analysis of IL-6, IL-1β and TNF-α production in monocytes isolated from multiple sclerosis patients treated with disease modifying drugs *J. Syst. Integr. Neurosci.* 2017; Vol. 3 3.
(23) Cadden, J.; Gupta, K. M.; Kanaujia, P.; Coles, S. J.; Aitipamula, S. Cocrystal Formulations: Evaluation of the Impact of Excipients on Dissolution by Molecular Simulation and Experimental Approaches. *Cryst. Growth Des.* **2021**, *21*, 1006−1018.
(24) Allu, S.; Suresh, K.; Bolla, G.; Mannava, M. K. C.; Nangia, A. Role of hydrogen bonding in cocrystals and coamorphous solids: indapamide as a case study. *CrystEngComm* **2019**, *21*, 2043−2048.
(25) Cuadra, I. A.; Cabañas, A.; Cheda, J. A.; Martinez-Casado, F. J.; Pando, C. Pharmaceutical co-crystals of the anti-inflammatory drug diflunisal and nicotinamide obtained using supercritical CO2 as an antisolvent. *J. CO2 Util.* **2016**, *13*, 29−37.
(26) Cao, Y.; Mu, T. Comprehensive investigation on the thermal stability of 66 ionic liquids by thermogravimetric analysis. *Ind. Eng. Chem. Res.* **2014**, *53*, 8651−8664.
(27) Liu, X.; Lu, M.; Guo, Z.; Huang, L.; Feng, X.; Wu, C. Improving the chemical stability of amorphous solid dispersion with cocrystal technique by hot melt extrusion. *Pharm. Res.* **2012**, *29*, 806−817.
(28) Sarkar, A.; Rohani, S. Cocrystals of acyclovir with promising physicochemical properties. *J. Pharm. Sci.* **2015**, *104*, 98−105.
(29) Saganowska, P.; Wesolowski, M. DSC as a screening tool for rapid co-crystal detection in binary mixtures of benzodiazepines with co-formers. *J. Therm. Anal. Calorim.* **2018**, *133*, 785−795.
(30) Park, B.; Yoon, W.; Yun, J.; Ban, E.; Yun, H.; Kim, A. Emodin-nicotinamide (1: 2) cocrystal identified by thermal screening to improve emodin solubility. *Int. J. Pharm.* **2019**, *557*, 26−35.
(31) Ervasti, T.; Aaltonen, J.; Ketolainen, J. Theophylline−nicotinamide cocrystal formation in physical mixture during storage. *Int. J. Pharm.* **2015**, *486*, 121−130.
(32) Mao, C.; Childs, S. L. Cocrystals of dimethyl fumarate, 2016.
(33) Chadha, R.; Saini, A.; Jain, D. S.; Venugopalan, P. Preparation and solid-state characterization of three novel multicomponent solid forms of oxcarbazepine: Improvement in solubility through saccharin cocrystal. *Cryst. Growth Des.* **2012**, *12*, 4211−4224.
(34) Shen, J. P.; Duan, X. H.; Luo, Q. P.; Zhou, Y.; Bao, Q.; Ma, Y. J.; Pei, C. H. Preparation and characterization of a novel cocrystal explosive. *Cryst. Growth Des.* **2011**, *11*, 1759−1765.
(35) S G, P.; Echanur, A. V.; Matadh, A. V.; Rangappa, S.; H N, S.; Murthy, R. N.; V S, R.; Ureña-Benavides, E. E.; Maibach, H.; Murthy, S. N. Sublimation of Drugs from the Site of Application of Topical Products. *Mol. Pharmaceutics* **2023**, *20*, 2814−2821.
(36) Zu, H.; Henry, R. F.; Zhang, G. G. Z.; MacGillivray, L. R. Inhibiting Sublimation of Thymol by Cocrystallization. *J. Pharm. Sci.* **2023**, *112*, 350−353.
(37) Maheshwari, C.; André, V.; Reddy, S.; Roy, L.; Duarte, T.; Rodríguez-Hornedo, N. Tailoring aqueous solubility of a highly soluble compound via cocrystallization: effect of coformer ionization,

https://doi.org/10.1021/acsomega.3c02463
ACS Omega 2023, 8, 26218−26230

pH max and solute−solvent interactions. *CrystEngComm* **2012**, *14*, 4801−4811.
(38) Moharregh-Khiabani, D.; Blank, A.; Skripuletz, T.; Miller, E.; Kotsiari, A.; Gudi, V.; Stangel, M. Effects of fumaric acids on cuprizone induced central nervous system de-and remyelination in the mouse. *PLoS One* **2010**, *5*, No. e11769.
(39) Perpétuo, G. L.; Chierice, G. O.; Ferreira, L. T.; Fraga-Silva, T. F. C.; Venturini, J.; Arruda, M. S. P.; Bannach, G.; Castro, R. A. E. A combined approach using differential scanning calorimetry with polarized light thermomicroscopy in the investigation of ketoprofen and nicotinamide cocrystal. *Thermochim. Acta* **2017**, *651*, 1−10.
(40) Abdelrahman, R. S.; Abdel-Rahman, N. Dimethyl fumarate ameliorates acetaminophen-induced hepatic injury in mice dependent of Nrf-2/HO-1 pathway. *Life Sci.* **2019**, *217*, 251−260.
(41) Doganay, S.; Budak, O.; Sahin, A.; Bahtiyar, N. Antioxidant and Anti-Infl ammatory Eff ects of Nicotinamide Adenine Dinucleotide (NAD+) Against Acute Hepatorenal Oxidative Injury in An Experimental Sepsis Model *Kafkas Üniversitesi Veteriner Fakültesi Dergisi* 2022; Vol. *28*, 1, 121−132.
(42) Fang, H.; Liu, A.; Sun, J.; Kitz, A.; Dirsch, O.; Dahmen, U. Granulocyte colony stimulating factor induces lipopolysaccharide (LPS) sensitization via upregulation of LPS binding protein in rat. *PLoS One* **2013**, *8*, No. e56654.
(43) Wilms, H.; Sievers, J.; Rickert, U.; Rostami-Yazdi, M.; Mrowietz, U.; Lucius, R. Dimethylfumarate inhibits microglial and astrocytic inflammation by suppressing the synthesis of nitric oxide, IL-1β, TNF-α and IL-6 in an in-vitro model of brain inflammation. *J. Neuroinflammation* **2010**, *7*, No. 30. Ungerstedt, J.; Blombäck, M.; Söderström, T. Nicotinamide is a potent inhibitor of proinflammatory cytokines. *Clin. Exp. Immunol.* **2003**, *131*, 48−52.
(44) Heeba, G. H.; Hassan, M. K. A.; Amin, R. S. Gastroprotective effect of simvastatin against indomethacin-induced gastric ulcer in rats: role of nitric oxide and prostaglandins. *Eur. J. Pharmacol.* **2009**, *607*, 188−193.
(45) Rocha, B. S.; Lundberg, J. O.; Radi, R.; Laranjinha, J. Role of nitrite, urate and pepsin in the gastroprotective effects of saliva. *Redox Biol.* **2016**, *8*, 407−414.
(46) Palmer, R. M. J.; Moncada, S. A novel citrulline-forming enzyme implicated in the formation of nitric oxide by vascular endothelial cells. *Biochem. Biophys. Res. Commun.* **1989**, *158*, 348−352.
(47) Morris, G. M.; Goodsell, D. S.; Huey, R.; Hart, W. E.; Halliday, S.; Belew, R.; Olson, A. J. AutoDock. In *Automated Docking of Flexible Ligands to Receptor-User Guide*; Citeseer, 2001. Huey, R.; Morris, G. M.; Forli, S.Using AutoDock 4 and AutoDock vina with AutoDockTools: a tutorial *The Scripps Research Institute Molecular Graphics Laboratory* 2012; Vol. *10550*, p 92037.
(48) Studio, D. Discovery Studio. *Accelrys [2.1]* 2008.
(49) Ganeshpurkar, A.; Singh, R.; Kumar, D.; Divya; Shivhare, S.; Kumar, A.; Singh, S. K. Computational binding study with α7 nicotinic acetylcholine receptor of Anvylic-3288: an allosteric modulator. *Mol. Simul.* **2020**, *46*, 975−986.
(50) Le Grand, S.; Götz, A. W.; Walker, R. C. SPFP: Speed without compromise—A mixed precision model for GPU accelerated molecular dynamics simulations. *Comput. Phys. Commun.* **2013**, *184*, 374−380. Götz, A. W.; Williamson, M. J.; Xu, D.; Poole, D.; Le Grand, S.; Walker, R. C. Routine microsecond molecular dynamics simulations with AMBER on GPUs. 1. Generalized born. *J. Chem. Theory Comput.* **2012**, *8*, 1542−1555. Salomon-Ferrer, R.; Gotz, A. W.; Poole, D.; Le Grand, S.; Walker, R. C. Routine microsecond molecular dynamics simulations with AMBER on GPUs. 2. Explicit solvent particle mesh Ewald. *J. Chem. Theory Comput.* **2013**, *9*, 3878−3888.
(51) Sarraguça, M. C.; Paisana, M.; Pinto, J.; Lopes, J. A. Real-time monitoring of cocrystallization processes by solvent evaporation: A near infrared study. *Eur. J. Pharm. Sci.* **2016**, *90*, 76−84.
(52) Kumar, S.; Nanda, A. Pharmaceutical Cocrystals: An Overview. *Indian J. Pharm. Sci.* **2018**, *79*, 858−871.
(53) Buanz, A. B.; Parkinson, G. N.; Gaisford, S. Characterization of carbamazepine-nicatinamide cocrystal polymorphs with rapid heating DSC and XRPD. *Cryst. Growth Des.* **2011**, *11*, 1177−1181.
(54) Batisai, E.; Ayamine, A.; Kilinkissa, O. E. Y.; Báthori, N. B. Melting point−solubility−structure correlations in multicomponent crystals containing fumaric or adipic acid. *CrystEngComm* **2014**, *16*, 9992−9998.
(55) Weast, R. C.; Astle, M. J. *CRC Handbook of Chemistry and Physics*, 64th ed.; CRC: Boca Raton, 1984.
(56) Litjens, N. H. R.; Burggraaf, J.; van Strijen, E.; van Gulpen, C.; Mattie, H.; Schoemaker, R. C.; van Dissel, J. T.; Thio, H. B.; Nibbering, P. H. Pharmacokinetics of oral fumarates in healthy subjects. *Br. J. Clin. Pharmacol.* **2004**, *58*, 429−432.
(57) Danieli, P. P.; Ronchi, B.; Rossi, C. Assessing the in vitro viability of bovine peripheral blood mononuclear cells (PBMCs): a comparison between the MTT (or XTT) and Trypan Blue Exclusion (TBE) test. *Acta Nat. Sci.* **2014**, *1*, 58−61.
(58) Jedrzejewski, T.; Wrotek, S.; Piotrowski, J.; Kozak, W. Silver nanoparticles augment releasing of pyrogenic factors by blood cells stimulated with LPS. *Open Life Sci.* **2014**, *9*, 1058−1067.
(59) Noosud, J.; Lailerd, N.; Kayan, A.; Boonkaewwan, C. In vitro and in vivo assessment of inhibitory effect of stevioside on pro-inflammatory cytokines. *Avicenna J. Phytomed.* **2017**, *7*, No. 101.
(60) Chauhan, P. S.; Singh, D. K.; Dash, D.; Singh, R. Intranasal curcumin regulates chronic asthma in mice by modulating NF-κB activation and MAPK signaling. *Phytomedicine* **2018**, *51*, 29−38.
(61) Paliwal, P.; Dash, D.; Krishnamurthy, S. Pharmacokinetic study of piracetam in focal cerebral ischemic rats. *Eur. J. Drug Metab. Pharmacokinet.* **2018**, *43*, 205−213.
(62) Gold, R.; Schlegel, E.; Elias-Hamp, B.; Albert, C.; Schmidt, S.; Tackenberg, B.; Xiao, J.; Schaak, T.; Salmen, H. C. Incidence and mitigation of gastrointestinal events in patients with relapsing−remitting multiple sclerosis receiving delayed-release dimethyl fumarate: a German phase IV study (TOLERATE). *Ther. Adv. Neurol. Disord.* **2018**, *11*, No. 1756286418768775. Palte, M. J.; Wehr, A.; Tawa, M.; Perkin, K.; Leigh-Pemberton, R.; Hanna, J.; Miller, C.; Penner, N. Improving the gastrointestinal tolerability of fumaric acid esters: Early findings on gastrointestinal events with diroximel fumarate in patients with relapsing-remitting multiple sclerosis from the phase 3, open-label EVOLVE-MS-1 Study. *Adv. Ther.* **2019**, *36*, 3154−3165.
(63) Wang, J. P.; Yamasaki, S.; Takeuchi, K.; Okabe, S. Delayed healing of acetic acid-induced gastric ulcers in rats by indomethacin. *Gastroenterology* **1989**, *96*, 393−402.
(64) Xue, Z.; Shi, G.; Fang, Y.; Liu, X.; Zhou, X.; Feng, S.; Zhao, L. Protective effect of polysaccharides from Radix Hedysari on gastric ulcers induced by acetic acid in rats. *Food Funct.* **2019**, *10*, 3965−3976.
(65) Yang, X.; Xue, Z.; Fang, Y.; Liu, X.; Yang, Y.; Shi, G.; Feng, S.; Zhao, L. Structure−immunomodulatory activity relationships of Hedysarum polysaccharides extracted by a method involving a complex enzyme combined with ultrasonication. *Food Funct.* **2019**, *10*, 1146−1158.
(66) Sastry, K. V. H.; Moudgal, R. P.; Mohan, J.; Tyagi, J. S.; Rao, G. S. Spectrophotometric determination of serum nitrite and nitrate by copper−cadmium alloy. *Anal. Biochem.* **2002**, *306*, 79−82.

https://doi.org/10.1021/acsomega.3c02463
ACS Omega 2023, 8, 26218−26230